

ARTICLE

## On the Profiling of Air Leakage Infiltration Pattern across Chinese Vernacular Buildings

Samuel I. Egwunatum<sup>1\*</sup>, Udubra E. Akpezi<sup>2</sup>, Osamudiamen K. Otasowie<sup>1</sup>, Imole A. Awodele<sup>3</sup>

<sup>1</sup> Department of Quantity Surveying, Federal University of Technology, Owerri, 460114, Nigeria

<sup>2</sup> Department of Civil Engineering, Delta State University of Science and Technology, Ozoro, 334113, Nigeria

<sup>3</sup> Department of Quantity Surveying, Durban University of Technology, Durban, 4000, South Africa

### ABSTRACT

The purpose of this paper is to provide understanding of the seasonal pattern of air leakage (infiltration) in Chinese vernacular buildings across China's five climate regions. In achieving the set purpose, a grand extensive literature survey was conducted and supported with data drawn from established Meteorom V6.1 on sensible heat and psychrometric variables. Numerical computations for normalized and specific infiltration from stack effects followed the Gowri method in line with ASHRAE reference 2004. Solar energy admittance into building followed Bouger's model form Angstrom properties. From the distribution of vernacular buildings across five climate regions of China, evidence from computational and numerical values showed symmetries in terms of minimums and maximums times of occurrence. Further, a reciprocal pattern exists between solar radiative admittance and region's temperature profile. Knowing that Chinese vernacular building heritage extended to further Asia, this research became limited to only the Chinese region. It became difficult to report if the construction culture away from China has correlation with infiltration and energy admittance value. Earlier works on Chinese climate and vernacular dwellings reported a climate responsive dwelling designed by passive cooling strategy; a gap was closed by extending the previous work to specific infiltration pattern and energy admittance level. Chinese vernacular buildings by virtue of research outcomes are and should be adoptable to modern housing needs for cultural integration.

**Keywords:** Infiltration; Vernacular building; Seasonal pattern; Psychrometric; Solar radiation; Admittance

#### \*CORRESPONDING AUTHOR:

Samuel I. Egwunatum, Department of Quantity Surveying, Federal University of Technology, Owerri, 460114, Nigeria; Email: [samuelegwunatum@gmail.com](mailto:samuelegwunatum@gmail.com)

#### ARTICLE INFO

Received: 23 February 2023 | Revised: 21 March 2023 | Accepted: 27 April 2023 | Published Online: 19 May 2023

DOI: <https://doi.org/10.30564/jsbct.v5i1.5490>

#### CITATION

Egwunatum, S.I., Akpezi, U.E., Otasowie, O.K., et al., 2023. On the Profiling of Air Leakage Infiltration Pattern across Chinese Vernacular Buildings. *Journal of Smart Buildings and Construction Technology*. 5(1): 29-51. DOI: <https://doi.org/10.30564/jsbct.v5i1.5490>

#### COPYRIGHT

Copyright © 2023 by the author(s). Published by Bilingual Publishing Group. This is an open access article under the Creative Commons Attribution-NonCommercial 4.0 International (CC BY-NC 4.0) License. (<https://creativecommons.org/licenses/by-nc/4.0/>).

# 1. Introduction

Chinese architecture as exemplified in their vernacular buildings is inseparable from Chinese civilization. There are literature and contextual graphics to assert and differentiate Chinese indigenous architecture as different from Roman, French and English architecture on face value [1-3]. Chinese architecture has shown consistency with regards to the conservative properties of their geometries and materials used in achieving them. Common vernacular elements such as quadrangles (enclosed spaces) parallel and bilateral symmetries, horizontal emphasis, and their attachments to allegorical representations in terms of cosmic energies, myth and dirge of ancestral mindedness are sure and common features of Chinese vernacular architecture [4-6]. It is not uncommon to classify these vernacular buildings into palaces, worship centers or monuments and pagodas to show homogeneity. Several literature exits to emphasize that Chinese vernacular buildings portray seeming unifying congruencies of variation with respect to owner’s status and affiliation like emperor’s buildings, religious buildings, public use and low-class society owner [7-9]. As a form of variants not necessarily on the basis of status and affiliation, there are classifications linked to geographic and regional narratives on the ethnic sense and yearly temperature profiles [10]. While we allude the historicity of Chinese vernacular buildings, it is important to draw from their architectur-

al heritages regarding what they offer to modern homes through historic introspection of their extreme weather responses and adaptive strategies. Such history metrics present us with historical retention worth and commercial value addition when such heritage architecture offers construction mimicking a copious adaptive technology [11-13]. In the light of this introduction, this paper sets out to assess the question of climate impact on occupants and the fitting energy admittance profile owing to Chinese architectural conceptualization in their vernacular building designs.



# 2. Literature review





There are strong sympathies in the architectural and construction world as typified in many learned society’s special issue journals to document and preserve by academic research, historic and heritage buildings such as Chinese vernacular buildings that are fast disappearing by the influence of time and technological development [14]. Though Chinese vernacular buildings are struggling for relevance and preservation with the demand of modern architecture, it has been shown that monument buildings and the composite materials used in their construction, together with their outdoor conditions have insignificant effect on the indoor temperature and humidity [15]. Architectural descriptive anthology of Chinese vernacular buildings was illustrated [16,17].

**Table 1.** Types and characteristics of Chinese vernacular buildings.

S/N	Type	Characteristics
1	<p><i>Siheyuan</i></p> 	<p>Vary in size and design                      Arrayed in rows                      High class Siheyuan owners are built with roof beams and pillars beautifully carried and painted with the luxury of back and front yards                      Specially built Siheyuan are south facing to enable sunshine admittance and resist cold wind from the north</p>

Table 1 continued

S/N	Type	Characteristics
2	<p><i>Tulou</i></p> 	<p>The WufengTulous are modernized forms of the Chinese courtyard construction system by the Hakkas They are typified with three halls and two side rooms The earth walls of WufengTulous 4 sides form enclosures and often act as defensive fortress and forte</p> <p>The side rooms are heightened wing rooms to reinforce the courtyard</p>
3		<p>The rectangular Tulou by historic facts appears to be earlier than the Wufeng and round Tulou buildings Typical of Chinese architecture, the three (3) types of the Tulou buildings have the same architectural informatics varying only in geometricity</p> <p>The rectangular Tulou dates back to 600 years ago often called WuyunTulou by the natives of the Northern part of Guzhu, Yongding</p> <p>The round Tulou is more complex than the rectangular and WufengTulous owing to the infiltration of Westernization ideas in their architectural reforms</p> <p>The round Tulou have their first appearance about 300 years ago</p> <p>They are divided into small, medium and large round Tulou types. Small round Tulou is about two or three storey heigh, consisting of a single ring. Medium Tulous have three to four storey-heights with wider diameters/two rings. Larger Tulous have four to five storeys with two/three rings. The most distributed round Tulous are the medium ones. The Tulous are often occupied and often used to emphasize kindred, making it look like a mini village, than more of a single building</p> <p>Round Tulou are characterized by a single fortified door with a foyer behind the door though not the only major access but also public space for the occupants It has ideal natural ventilation with the same room sizes for any type of round Tulou at the same location on each floor and with kitchen always at the ground floor. They have small windows which open to the outside</p>

S/N	Type	Characteristics
4	<p><i>Stone Dwellings</i></p> 	<p>The three outside walls are built with stones The wooden roof is covered by stone slabs The material and construction type makes it affordable and protect against the wind and rain</p>
5	<p><i>Cave Dwelling</i></p> 	<p>This type of construction method helps in economizing materials etched from stone carvings The shapes of the cave-dwelling houses make indoor temperature regulated by keeping warm in winter and cool in summer</p>
6	<p><i>Shanxi Folk House/ Jiangsu Folk House</i></p> 	<p>The houses are set up with patio. They have a spacious hall to insulate the heat and keep off the rain.</p>
7	<p><i>Shanghai Shikumen Dwelling</i></p> 	<p>They mostly feature stone gate frames with slack thick solid wood gates.</p>

Investigation between the interface of China’s climate and its vernacular buildings with the aim of adapting the traditional climate response architecture into modern residential development has seen tendencies for the Chinese design philosophy [18-20]. Attempts made by the Chinese government towards technological development for sustainable buildings with energy-saving potentials have resorted to mimicking the vernacular style of architecture as a response mechanism towards mitigating energy crises in the region [21-23]. Chinese vernacular buildings are notable for brought about energy-balancing construction materials and architectural designs, an adaptive response strategy in balancing thermal comfort between the extremes of winter and summer [24]. Evidence of Chinese vernacular buildings distributed across China shows that two-thirds of the buildings are hosted in one-third of the cold region of China. Referring to the study, China was partitioned into five climatic regions: cold region, moderate region, hot summer and cold winter region and hot summer and mid-winter region [18]. The two-thirds distribution of these vernacular buildings with variations is reported to be across Shanxi, Lingnan, Minnan, Hakka, Gan, Yaodong, Tibet, Xinjiang, and others [23,25-27]. Owing to the geographic metric of latitudinal variation, the climatic differentials across subarctic to tropical regions of vernacular building thermal comfort adaptive strategies deployed into modern architecture have shown fitting adoptable efficient potential of ventilation, air tightness, thermal capacity, passive solar gains and passive solar controls [28-31]. Comparative temperature and psychrometric measurements across these regions with the intent of reporting vernacular building air leakage profile are in this study reproduced for extended treatment [18]. Adopting the integration of modern architecture into China’s vernacular idea of buildings has shown promise of energy balance in buildings that have spurred technological research towards having green or zero energy buildings that call for overthrowing the use of fossil energy plants to cooling/heating buildings with attendant high cost [5,11,32,33]. Modern design re-

sponses to thermal discomfort in buildings are replete with passive cooling and heating systems [34] itemized four adaptive passive cooling actions to include storing capability/potential, avoidance, removal of undesirable heat gain and slow absorptivity of passive cooling materials. It required that passive cooling material should have the potential to store cold air within the building envelope, avoid or repel direct external solar radiation heat gain, remove heat gained from interior or exterior sources and slow/damp heat transferred from external climate through the building envelope [35-38]. The benefit of passive actions can be attained by the following remediation measures enumerated.

**Table 2.** Passive cooling potentials in the building.

S/N	Passive Action	Remediation Means
1.	Storing	Keeping cold air away from direct heat gains before gaining entrance into interior areas like basements, courtyards, thermal/heating areas and earthen spaces.
2.	Avoidance	Repelling external heat gain by using reflective/shading glazed windows/walls, reflective colors and irregular wall geometries to diffuse solar transmittance.
3.	Removal	Extraction of heat gained into the building from exterior and interior sources by controlled ventilation by the integration of wind flowers, earth lined tunnels and ventilation supported winds in designs.
4.	Slowing	Damping-off heat transferred from the external climate through the building envelope using double-glazed window unit and heat insulators.

### 3. Vernacular buildings physics

The thought of buildings being green conformed is us situated in their ability to maintain the balance between heating and cooling loads moderated into and out of the building by a certain “Maxwell’s demon” towards occupants’ desired comfort. The supply and removal of such thermal energy flow as a thermodynamic process requires the estimation of building performance at peak loading points [39-41]. Bearing in mind that Chinese vernacular buildings largely depend on outsourcing of their energy

demand in addition to indoor man-made carbon source energy uses in their energy balance strategy. A recourse to their climatic conditions will to a reasonable extent account for their thermal energy sustainability plan in retrospect. Analyzing energy requirements and balance in Chinese vernacular buildings calls for the amount and pattern of building air exchange in terms of infiltration and ventilation for controlled and uncontrolled situations to be appraised. The industry is quite familiar with ASHRAE indoor occupants' comfort recommendations related to the equation:

$$Q + W = MA_{sk} \quad (1)$$

$A_{sk}$  = total surface area of skin,  $M$  = rate of metabolic energy production per skin surface area,  $Q$  = production rate of heat,  $W$  = production rate of work. Considering the occupant comfort function above, we can draw congruencies with vernacular building infiltration and ventilation link to the airflow through openings in proportion to the building area and to some degree of the pressure difference <sup>[30,42]</sup>:

$$\dot{V} = A_c \Delta p^n \quad (2)$$

We assign  $A$  = area of opening ( $m^2$ ),  $\Delta p = p_0 - p_1$  = pressure difference (outside of building and inside of building),  $c$  = flow coefficient ( $m/s \cdot Pa^n$ ),  $n$  = degree/exponent of pressure between 0.4 to 1.0. To a large extent, cracks outside of vernacular buildings have been consistent with Lydberg and Honarbakhsh experiment. It has been reported to be compressible by external pressures given rise to reduced leakage area <sup>[43]</sup>. With the incidences of over pressurization and under pressurization at particular times of the year, total flow is obtainable by summing all leakage points  $K$ :

$$\dot{V} = \sum_k A_k C_k \Delta P_k^{n_k} \quad (\text{provided } \Delta P_k > 0) \quad (3)$$

We assign  $A_k$  = leakage area,  $C_k$  = flow coefficient,  $n_k$  = power exponent,  $\Delta P_k = p_0 - p_1$  = locally traceable pressure difference provided  $p_0 > p_1$ . Mostly, the pressure difference associated with vernacular buildings is deducible from three sources, enabling  $\Delta p = p_0 - p_1$  been linked by the sum of the following sources:

$$\Delta P = \Delta P_{wind} + \Delta P_{stack} + \Delta P_{vent} \quad (4)$$

Following the ability to compute separately for the three individual terms owing to non-linear flow with the variation of flows across the vernacular envelope, we attribute the total air pressure difference to the sum of the individual term differences <sup>[44]</sup>. However, the wind pressure is accountable by Bernoulli's Steadystate equation.

$$P_{wind} = \frac{\rho}{2}(v^2 - v_f^2) \quad (5)$$

with  $v$  = wind speed ( $m/s$ ),  $v_f$  = final speed of air at building boundary,  $\rho$  = air density  $kg/m^3$ . So that at the inner leaf of the wall entering the building, the local pressure difference approximately approaches:

$$\Delta P_{wind} = \Delta C_p \frac{\rho}{2} v^2 \quad (6)$$

with  $\Delta C_p = C_p - (-0.2)$  due to the difference between the local pressure coefficient and the average. There are situations where there is a density difference between outside and inside air in buildings. Vernacular buildings have the potential to maintain warmer air inside with less density than outside air leading to the pressure difference between outside and inside in winter needing heating. This process is reversed for the cooling season when indoor air is colder than the outside. Given this scenario, such pressure difference vernacular buildings are accounted for by:

$$\Delta P_{stack} = -C_d \frac{\rho_i g}{g_c} \Delta h \frac{T_i - T_o}{T_o} \quad (7)$$

$\rho_i$  = density of air in building = ( $1.20 \text{ kg/m}^3$ ),  $\Delta h$  = vertical distance from neutral pressure level,  $g = 9.8 \text{ m/s}^2$ ,  $T_i$  and  $T_o$  = indoor and outdoor absolute temperature ( $k$ ),  $C$  = draft coefficient, a dimensionless number to account for the resistance to airflow between doors. Idealizing the law of conservation of mass, we reason that the net airflow occasioned by ventilation in vernacular buildings equals the net leakage  $\dot{V}$  of sites ( $k$ ) of the envelope:

$$\dot{V} = \sum A_k C_k \Delta P_k^{n_k} \quad (8)$$

Arising from  $\Delta P_k = \Delta P_{wind,k} + \Delta P_{stack,k} + \Delta P_{vent}$ , if  $n \rightarrow 1$ , then,  $\Delta P_k^n = \Delta P_{vent}^n (1 + x_k)^n$ :

$$\text{where } x_k = \frac{\Delta P_{wind,k} + \Delta P_{stack,k}}{\Delta P_{vent}}$$

$$\text{then } \dot{V}_{vent} = \Delta P_{vent}^n \sum A_k C_k \left[ 1 + nx_k + \frac{n(n-1)}{2} x_k^2 + \dots \right] \quad (9)$$

Lawrence Berkeley Laboratory method based on the air pressurization test of buildings known as LBL model for determining airflow ( $V$ ) in buildings once the total leakage area has been determined are similar for Vernacular buildings obtainable from:

$$\dot{V} = A_{leak} \sqrt{a_s \Delta T + a_w v^2} \quad (10)$$

$A_{leak}$  = total effective leakage area of building,  $\text{cm}^2$ ,  $a_s$  = stack coefficient from ASHRAE table,  $\Delta T = T_i - T_o$ , (k),  $a_w$  = wind coefficient from ASHRAE table,  $v$  = average wind speed, m/s. Heat transmission potentials from outdoor temperature to indoor in Chinese vernacular buildings are best annotated in checking for the heat balance by determining its heat flow across the envelope [45]. Bearing together, the total components of the envelope, and the total heat flow are obtained from the total conductive heat from the vernacular building interior to exterior [40,42,46].

$$\dot{Q}_{cond} = \sum_k U_k A_k (T_i - T_o), U = \text{conductance value} \quad (11)$$

For most appropriate case, it is unifying to obtain the total conductive heat transmission coefficient ( $k_{cond}$ ) for vernacular buildings by:

$$K_{cond} = \sum_k U_k A_k$$

So that for single section interior temperature ( $T_i$ ), the conductive heat flow is associated most appropriately as:

$$\dot{Q}_{cond} = K_{cond} (T_i - T_o)$$

In a more general and complicated interior, effective value is obtained by adding U-values for glazing, opaque walls and roof to obtain:

$$K_{cond} = U_{glaz} A_{glaz} + U_{wall} A_{wall} + U_{roof} A_{roof} \quad (12)$$

It is necessary to determine sensible heat due to air exchange for vernacular building energy balance for indoor occupants which is proportional to  $T_i - T_o$  and obtainable by:

$$\dot{Q}_{air} = pc_p \dot{V} (w_1 - w_o) \quad (13)$$

For which,  $p$  = density of air,  $c_p$  = specific heat of air,  $\dot{V}$  = air exchange rate. Taking the latent heat gain to the building from different sources and majorly

from solar exposure we appropriate:

$$\dot{Q}_{air, lat} = \dot{V} p h_{fg} (w_o - w_i) \quad (14)$$

$\dot{V}$  = volumetric air exchange rate ( $\text{m}^3/\text{s}$ ),  $p$  = density ( $\text{kg}/\text{m}^3$ ),  $ph_{fg} = [3010 \text{ w}/(\text{L}/\text{s})]$  at standard conditions,  $w_i, w_o$  = humidity ratios of indoor and outdoor air. On the basis of the transfer function protocol established by ASHRAE for determining conductive heat gain we as well deploy it to the measurement of conductive heat gain for vernacular buildings taking into account as being proportional to their loss in time (t) duration through walls and roof by:

$$\begin{aligned} \dot{Q}_{cond, t} = & - \sum_{n \geq 1} dn \dot{Q}_{cond, t} - n \Delta t \\ & + A (\sum_{n \geq 0} b_n T_{os, t} - n \Delta t - T_i \sum_{n \geq 0} c_n) \end{aligned} \quad (15)$$

where  $A$  = area of roof or wall ( $\text{m}^2$ ),  $\Delta t$  = time step = 1 h,  $T_{o, st}$  = sol-air temperature of outside surface at time 't'.  $b_n, c_n, d_n$  = coefficients of conduction transfer function, which under steady-state limit, having the boundary conditions of  $Q_{cond}$ ,  $T_{os}$  and  $T_i$  as all constant enables transfer function by U-values of:

$$U = \frac{\sum_{n \geq 0} c_n}{\sum_{n \geq 0} d_n} \quad (16)$$

Considering  $d_o = 1$  from relation  $\dot{Q}_{cond} \sum_{n \geq 0} d_n = A (T_{os} \sum_{n \geq 0} b_n - T_i \sum_{n \geq 0} c_n)$ .

## 4. Methodology

Obtaining the amount of infiltration in this paper deployed the use of computations for normalized leakages, volumetric flows, specific infiltration from stack effects and temperature differentials. Each vernacular architectural theme building followed a theoretical aggregated components opening for opaque and fenestration elements simulated at one square meter ( $1 \text{ m}^2$ ) less leakages between interfaces of components and workmanship for a baseline from ASHRAE SSPC90.1-2004. Envelope subcommittee Addendia 'Z' recommended value of 1.8 cfm/sf @0.3 in w.c. Air change rate (ACR) is computed from air normalized leakages and infiltration reference from ASHRAE Standard 2004. Numerical values obtained, follows, the method [47] on data ob-

tained from Meteorology V6.1 for: Air temperature, daily minimum and maximum temperature, relative humidity, irradiation of global radiation horizontal, irradiation of beam, sunshine duration on a daily and monthly basis, precipitation, days of precipitation, wind speed and wind direction feigning on data [18]. These data were mined from China's five (5) different climate regions which by Chinese authority documents distributed them as: Hot and cold winter region, hot and mild winter region, severe cold region, moderate region and cold region. The idea is to obtain the climatic distributive impact on vernacular buildings in terms of thermal comfort while introspecting their viability in terms of building elements' adaptations to modern architecture. Accordingly, data used were for areas with Siheyuan, Tulou, Shaikumen and Jiangsu Folk buildings. Concerning the amount of solar energy available to vernacular occupants in retrospect, profiling on a regional basis of beam solar irradiance is conducted to determine the energy amount per unit time per unit area admissible to the buildings in accordance with Bouger's model from Angstrom properties.

## 5. Results and discussions

In the international arena, there are guidelines for efficient building ventilation that tolerates air movements in and out with occupants' indoor air quality concerns. Such guidelines have been addressed by policy documents in European standards such as that for building energy performance in EN16798-17 (2017) building services regulation in EN15299 (2019), airflow measurements in buildings on the in-situ basis in EN16211 (2015) and building performance testing for insulation and ventilation systems in EN14134 (2004, revised 2019). On the contrary to Chinese vernacular buildings, natural adaptability control is used in strategic design openings and vertical air ducts are deployed in modern designs in the international arena by mechanical means of using heat recuperation exchangers and humidity control. Whether Chinese vernacular buildings are green conformal, is responded to with semblance of some of Europe's nZEB regulations documents. In France,

RT 2012 regulations provide for the "13Bio" index to evaluate the impact of bio-climatic designs on building energy performance from the relationship.

$$Bbio = ZE_{heat} + ZE_{cooling} + 5E_{lighting}$$

{criterion measurement;  $Bbio < Bbiomax 2012$ }.

Since RT 2012 policy document, compliance with criterion estimate has become a necessary condition for building development across Europe. The nZEB criterion which is possessed by vernacular buildings is that buildings should possess energy efficiency rate of 40-60 Kwh/yr/m<sup>2</sup> for buildings not less than 42° South and 72° North which shows symmetry with the RT2012 policy document. Taking into cognizance the prerequisites for air leakages, a corroboration was drawn in this paper to be consistent with the requirements that cracks/holes and air-pressured surfaces are fundamental to air leakages, with respect to vernacular buildings [40,47,48]. In this paper, we have attributed our leakage operative force to wind, originating from atmospheric/weather conditions and stack effects resulting from vertical (ground to height, H) movement of air pressure occasioned by air buoyancy. The understanding is that, wind into a vernacular building envelope act as a source of pressure differentials which manifest in infiltration been a property of wind speed and duration from high-pressure areas of wind routes to the building. The process is in proportion to the ratio of wind speed ( $W_{sp}$ ) at the building roof and the average impinging on the building surface ( $W_{avg}$ ) related by the ratio product.

$$\frac{W_{sp}}{W_{avg}} = \left(\frac{\delta_{met}}{H_{met}}\right)^{\alpha_{met}} \left(\frac{H_{bldg}}{\delta_{bldg}}\right)^{\alpha_{bldg}} \quad (17)$$

where  $\alpha, \delta$  are parametric evaluators of wind boundary layer height and a corresponding exponent. Averaging  $\alpha, \delta$  over the building height (H), an impinging average over height to bottom of the building's wind speed from the relation.

$$\frac{W_{sp}}{W_{met}} = \frac{1}{H_{bldg}^{\alpha_{bldg}+1}} \frac{1}{\left(\frac{1}{\delta_{bldg}}\right)^{\alpha_{bldg}}} \left(\frac{\delta_{met}}{H_{met}}\right)^{\alpha_{met}} \left(\frac{H_{bldg}}{\delta_{bldg}}\right)^{\alpha_{bldg}+1} \quad (18)$$

Thermal profiling on a regional basis showed that Chinese vernacular buildings according to latitudinal variation have shown adequate responsive dwelling



design strategies <sup>[18]</sup>. Those buildings that have responded adequately to passive solar gains are those in the severe cold (see **Table 3**), hot summer and cold winter (see **Table 6**) and cold winter regions (see **Table 4**). Those that have shown adequate thermal capacity are buildings in severe cold, cold and hot summer and cold winter regions. Buildings also in severe cold, cold and hot summer and cold winter regions have demonstrated a capacity for air tightness. Passive solar controls are noticeable in buildings in cold, moderate, hot summer and cold winter and hot summer and warm winter regions. Ventilation adequacy was reported for buildings in hot summer and cold winter (see **Table 6**), hot summer and warm winter (see **Table 7**), moderate and cold regions (see **Table 5**). As follow-up to these observations this paper additionally reports the infiltration properties of these buildings across regional divides. Our observation is that infiltration in the hot summer and mild winter Haikou region is maximum in November and December of the year and lowest in September. In the hot summer and cold Wuhan regions, infiltration is maximum in August of the year and lowest in November of the year. The Harbin region of severe cold has its highest infiltration in April of the year and lowest in August of the year. The cold region profile at Beijing shows that infiltration is highest in March and lowest in September and October periods of the year. Finally in the moderate region of Kunming infiltration is highest in April and lowest in September (see **Table 18**). The impact of environmental physics on building heating and cooling loads is indicated by the metrics of relative humidity, precipitation and windspeed. These metrics of indoor level are governed by the law of energy conservation by the terms, absorptivity ( $\alpha$ ), transmissivity ( $\tau$ ) and reflectivity ( $\rho$ ) been:

$$\alpha + \tau + \rho = 1$$

The various regions of Harbin 44.5°N (referring to **Tables 8 and 13**), Beijing 39.5°N (referring to **Tables 9 and 14**), Kunming 25°N (referring to **Tables 10 and 15**), Wuhan 30°N (referring to **Tables 11 and 16**) and Haikou 20°N (referring to **Tables 12 and 17**) hosting vernacular buildings have shown by their

windspeed, precipitation and relative humidity values in tandem with energy conservation law to have temperature admissibility pattern on yearly circle. Such seasonal temperature profile addresses indoor thermal comfort with an inverse relation to environment relative humidity and consequently justifies infiltration pattern in vernacular buildings (see **Figures 6-10** for windspeed profile). This on the contrary for precipitation shows a direct relationship with an increase in temperature necessitating more evaporating at homes (see **Figures 11-14**). Vernacular building occupants comfort is linked to humidity and temperature levels which are aided by outside air, bathroom water capillarity, indoor cooking devices and solar admittance in accordance with Equations (21) and (22) and experimentally supported <sup>[12,49]</sup>. The cycle of infiltration pattern in Chinese vernacular building types opting for an optimized design either by geographic accident or local science architecture in their cold/warm region, maintains the balance between cold and heat with adequate insulation and thermal delay heat peaks by damping. Humidity pattern fluctuation (rise and fall) in severe cold weather region profile showed three points in the year-round humidity cycle noticeably for rise in January, July and December (see **Figures 1 and 2**) at Harbin 44.4°N and Beijing 39.5°N. Three-point flexions are observed for moderate weather region air moisture content humidity for Kunming 25°N in January and July and slow unnoticeable drop till December (see **Figure 3**). The humidity pattern in the hot summer and cold winter profile suggests multiple flexural patterns almost unpredictable at Wuhan 30°N (see **Figure 4**) and same for Haikou 20°N (see **Figure 5**) for the hot summer and mid-winter region.

As an extension of work <sup>[18]</sup> by profiling for infiltration together with previous observations we report with the table below.

It is recursive to state that vernacular buildings with their native architectural design concepts and materials used in construction have predictable year-round infiltration (pattern) that allows for energy utilization plans. Secondly, given to the general reportage of temperature growth across the globe, oc-

caused by global warming, temperature differential at points  $T_0$  and  $T_1$  (outside and inside) vernacular buildings enables warm air in the envelope to rise upward as the air becomes buoyed. This effect drags cold air by the conventional current to the bottom of the building space in exchange for warmth that is expelled at the building's top most part. This often led to air leakage due to precipitation from moisture (see **Figures 12-15**). These occurrences are annotated  $\Delta_{at}$  together with the regional wind speed values at different times of the year which lends agency to infiltration. Wind speed maximums at different regions are illustrated in **Figures 7-11**. The observations are frequent mostly in Cold severe cold regions area in August with the highest point of precipitation at 60 mm. In cold regions, precipitations are still high in August with 182 mm value. Moderate regions still have their highest precipitation in August with 16 mm. Hot summer and Cold winter region precipitates 166 mm value in May while hot summer and mild winter region have longer time of precipitation with 12 mm values during the periods of May, June, August and September. These periods highlighted in all regions show times at which air leakage, being a condition for infiltration to vernacular buildings are prevalent (see **Tables 18 and 19**). In view of the vernacular building's thermal capacity, an investigation of the apparent solar energy admittance into the building based on Bouger's model was conducted.

$$I_{b, N} = I_e^{-\int k \cdot dx} \quad (19)$$

where  $x$  = length of travel through the atmosphere  $I_{b, N}$  = instant beam solar radiation per unit area normal to the sun's ray and used to related determine the amount of solar energy admittance to occupants following the amount of beam solar radiation arriving on those Chinese regions on account of the variously dispersed regional temperature profiles investigated for vernacular buildings <sup>[50,51]</sup>. Drawing from the ASHRAE model for this estimation, we have the beam component and diffuse component for solar irradiance as:

$$I_{b, N} = I(e^{-Ibm^b}) - beam \quad (20)$$

$$I_{b, N} = I(e^{-I dm^d}) - diffused$$

$I_{b, N}$  = Beam normal irradiance per unit area normal to sun rays,  $I_{d, H}$  = Diffused horizontal irradiance,  $m$  = air mass,  $I_b, T_d$  = Pseudo-optical depths with location parameters,  $b, d$  = Beam and diffuse air mass exponents. Noting that  $i$  is the angle of arrival or incidence of beam radiation on vernacular wall surface, the instantaneous solar energy admittance or beam radiation on the wall Impact area was obtained from:

$$I_{b, c} = I_{b, N} \text{Cos}i$$

Following the flagellating occurrence of such irradiance, we deployed the monthly value estimation for yearly basis passiveness for occupants <sup>[21]</sup>. In these circumstances, we resort to the Angström linear model estimation parametrized by average horizontal radiation to clear day radiation and related to the sunshine level as a percentage of possible hours of sunshine <sup>[52]</sup>.

Given the Angström model:

$$\begin{aligned} \bar{H}_h &= \bar{H}_{o, h} \left( a + b \frac{\bar{n}}{\bar{N}} \right) \\ &= \bar{H}_{o, h} \left( a + b \frac{\bar{P}\bar{S}}{100} \right) \end{aligned}$$

$\bar{H}_h$  and  $\bar{H}_{o, h}$  are horizontal terrestrial and horizontal extraterrestrial radiation levels average for a month.  $\bar{P}\bar{S}$  is the monthly average percentage of possible sunshine, 'a' and 'b' are constants for a given region,  $\bar{N}$  and  $\bar{n}$  are monthly average numbers of hours of daylight and bright sunshine <sup>[53]</sup>. The ratio  $\frac{\bar{n}}{\bar{N}} \equiv \frac{m}{m}$  monthly average percent sunshine (PS). In this case, we have:

$$H - B_n = H - a_h \left( a + b \frac{\sum_{i=1}^{30} SD_d}{100} \right) \quad (22)$$

Obtaining from the Computations of Angström-PreScott parameters for various regions of China's solar radiation estimation, we have the (a + b) values for the regressive functions:

- 1)  $a + b = 0.253Z + 0.7169$  (min. value)
- 2)  $a + b = 0.0262Z - 0.0101\text{Cos}\varphi + 0.067 \text{cos}\Phi + 0.7164$ . (max. value).

Such that their mean values are deployed for the various region yearly solar admittance from Equation (22) above.

**Table 3.** Severe cold region weather profile at Harbin (44.5°N).

Month	At	Ātmax	Ātmin	RH	H_Gh	H_Bn	SDm	SDd	PCt	Pctd	Wsp	Wdr	ΔAt
January	-17.1	-11.9	-21.2	71	52	93	177	5.7	7	0	2.4	11	9.3
February	-11.3	-5.7	-16.7	64	74	109	191	6.8	3	1	2.7	11	11
March	-2.2	3.2	-7.2	50	119	141	234	7.5	10	1	3.3	11	10.4
April	8.5	14.2	3.1	43	140	116	221	7.4	10	3	3.4	184	11.1
May	15.8	21.6	9.8	45	163	118	254	8.2	32	4	3.3	154	11.8
June	21.6	26.4	15.3	53	168	124	249	8.3	44	7	2.9	174	11.1
July	23.7	27.9	19.3	71	156	113	238	7.7	50	11	2.6	153	8.6
August	21.4	25.7	17.1	73	139	114	231	7.5	60	8	2.3	174	8.6
September	15.6	21	9.8	62	119	116	225	7.5	30	6	2.4	11	11.2
October	6.3	11.8	1.7	55	88	111	211	6.8	18	3	2.8	11	10.1
November	-5.1	-0.4	-9.1	61	56	93	176	5.9	7	1	2.7	11	8.7
December	-14.5	-9.5	-18.8	68	43	74	155	5	4	1	2.5	11	9.3

Source: Sun (2013).

**Table 4.** Severe cold region weather profile at Beijing (39.5°N).

Month	At	Ātmax	Ātmin	RH	H_Gh	H_Bn	SDm	SDd	PCt	Pctd	Wsp	Wdr	ΔAt
January	-3.4	-7.5	1.8	39	74	119	193	6.2	3	1	2.8	315	-9.3
February	0.6	-4.2	6	36	91	111	188	6.7	6	2	2.8	315	-10.2
March	7.1	1.9	12.8	36	132	132	235	7.6	9	2	3.1	315	-10.9
April	14.9	9.3	20.5	41	154	112	240	8	26	3	3	315	-11.2
May	20.7	14.9	26.4	49	184	121	276	8.9	29	4	2.8	295	-11.5
June	24.8	19.4	29.6	59	174	93	261	8.7	71	6	2.4	295	-10.2
July	27	22.7	31.5	70	155	79	219	7.1	176	10	2.1	90	-8.8
August	25.2	21.1	29.6	76	146	82	224	7.2	182	9	1.9	290	-8.5
September	20.7	15.6	25.7	66	132	105	236	7.9	49	4	2	290	-10.1
October	13	8.1	18.9	54	106	102	217	7	19	3	2.2	315	-10.8
November	4.6	0.2	9.7	50	73	94	185	6.2	6	1	2.4	315	-9.5
December	-1.4	-5.4	3.4	43	64	100	184	5.9	2	1	2.7	315	-8.8

**Table 5.** Moderate region weather profile at Kunming 25°N.

Month	At	Ātmax	Ātmin	RH	H_Gh	H_Bn	SDm	SDd	PCt	Pctd	Wsp	Wdr	ΔAt
January	9.5	4.4	15.3	58	115	141	222	7.2	22	2	2.4	279	-10.9
February	11.9	6.7	17.9	51	125	137	221	7.9	20	3	2.9	142	-11.2
March	15.2	10.1	21.1	47	159	142	255	8.2	30	3	3.2	142	-11
April	18.1	12.6	23.3	48	165	137	244	8.1	32	4	3.2	142	-10.7
May	19.2	14.9	23.6	60	154	97	214	6.9	90	9	2.8	142	-8.7
June	20.1	16.3	23.4	73	124	64	136	4.5	181	14	2.4	176	-7.1
July	20.1	17.1	23.3	78	121	63	139	4.5	175	16	2	142	-6.2
August	19.1	16.7	23.4	76	126	72	155	5	132	16	1.9	142	-6.7
September	18.2	14.5	21.8	72	112	82	135	4.5	80	12	2	279	-7.3
October	16.2	12.5	20.1	74	101	66	149	4.8	88	11	2.1	279	-7.6
November	12.4	7.9	17.1	69	100	99	172	5.7	29	5	2	279	-9.2
December	9.3	4.7	15	67	104	136	199	6.4	22	2	2.1	279	-10.3

**Table 6.** Hot summer and cold winter region weather profile at Wuhan (30°N).

Month	At	$\bar{A}t_{max}$	$\bar{A}t_{min}$	RH	H_Gh	H_Bn	SDm	SDd	PCt	Pctd	Wsp	Wdr	$\Delta At$
January	4.6	1.7	7.9	71	62	43	91	2.9	67	5	1.5	198	-6.2
February	7.6	4.2	11.2	68	67	29	80	2.9	63	6	1.6	23	-7
March	11.7	8.3	15.6	70	86	34	99	3.2	89	9	1.8	81	-7.3
April	18.2	14.1	22.1	70	107	40	122	4.1	135	11	1.9	81	-8
May	22.9	19.5	26.7	71	138	60	147	4.7	166	11	1.7	81	-7.2
June	26.5	22.9	29.3	75	135	49	160	5.3	171	10	1.7	81	-6.4
July	29.4	26.2	32.4	75	165	90	209	6.7	202	10	1.8	110	-6.2
August	28.2	25.3	31.4	76	150	87	213	6.9	117	10	1.9	81	-6.1
September	24.8	20.8	28.1	70	116	59	148	4.9	57	8	1.9	66	-7.3
October	18.6	15.1	22.4	71	93	57	132	4.3	80	8	1.6	66	-7.3
November	12.4	8.7	16.1	71	70	54	112	3.7	80	6	1.5	212	-7.4
December	6.4	3.3	10.3	70	62	44	101	3.3	39	4	1.6	198	-7

**Table 7.** Hot summer and mild winter region weather profile at Haikou (20°N).

Month	At	$\bar{A}t_{max}$	$\bar{A}t_{min}$	RH	H_Gh	H_Bn	SDm	PCt	Pctd	Wsp	Wdr
January	20.1	17.6	22.8	77	97	70	123	15	4	2.8	181
February	20.2	17.4	23.1	80	89	42	101	44	6	3	119
March	22.6	19.8	25.9	83	116	58	140	45	6	3.1	124
April	25.5	22.1	28.5	83	131	60	170	68	8	3.1	124
May	27.1	24	30.4	84	171	114	224	117	12	3	119
June	28.3	24.7	31.3	82	167	116	219	162	12	3	136
July	28.8	25.6	32.1	80	175	120	254	247	11	3	225
August	28.7	25.8	31.8	80	169	113	220	276	12	2.7	121
September	27.8	25.1	30.1	80	132	73	194	313	12	2.6	181
October	26.9	24.6	29.5	75	122	69	184	162	10	2.8	181
November	24.2	21.6	26.4	74	103	69	148	46	6	3	176
December	20.8	18.6	23.3	73	93	66	141	48	4	3	176

**Table 8.** Severe cold region windspeed profile at Harbin (44.5°N).

	$\Delta At$	$Fs^2$	$Fw^2$	$Ws_p^2$	$Fs^2, \Delta At$	$Fw^2, Ws_p^2$	S
January	9.3	0.0144	0.0174	5.76	0.13392	0.100224	0.48
February	11	0.0144	0.0174	7.29	0.1584	0.126846	0.53
March	10.4	0.0144	0.0174	10.89	0.14976	0.189486	0.58
April	11.1	0.0144	0.0174	11.56	0.15984	0.201144	0.60
May	11.8	0.0144	0.0174	10.89	0.16992	0.189486	0.59
June	11.1	0.0144	0.0174	8.41	0.15984	0.146334	0.55
July	8.6	0.0144	0.0174	6.76	0.12384	0.117624	0.49
August	8.6	0.0144	0.0174	5.29	0.12384	0.092046	0.46
September	11.2	0.0144	0.0174	5.76	0.16128	0.100224	0.51
October	10.1	0.0144	0.0174	7.84	0.14544	0.136416	0.53
November	8.7	0.0144	0.0174	7.29	0.12528	0.126846	0.50
December	9.3	0.0144	0.0174	6.25	0.13392	0.10875	0.49

**Table 9.** Severe cold region windspeed profile at Beijing (39.5°N).

	$\Delta At$	$Fs^2$	$Fw^2$	$Ws_p^2$	$Fs^2, \Delta At$	$Fw^2, Ws_p^2$	$S$
January	-9.3	0.0144	0.0174	7.84	-0.13392	0.136416	0.04
February	-10.2	0.0144	0.0174	7.84	-0.14688	0.136416	-0.10
March	-10.9	0.0144	0.0174	9.61	-0.15696	0.167214	0.10
April	-11.2	0.0144	0.0174	9	-0.16128	0.1566	-0.07
May	-11.5	0.0144	0.0174	7.84	-0.1656	0.136416	-0.17
June	-10.2	0.0144	0.0174	5.76	-0.14688	0.100224	-0.22
July	-8.8	0.0144	0.0174	4.41	-0.12672	0.076734	-0.22
August	-8.5	0.0144	0.0174	3.61	-0.1224	0.062814	-0.24
September	-10.1	0.0144	0.0174	4	-0.14544	0.0696	-0.28
October	-10.8	0.0144	0.0174	4.84	-0.15552	0.084216	-0.28
November	-9.5	0.0144	0.0174	5.76	-0.1368	0.100224	-0.19
December	-8.8	0.0144	0.0174	7.29	-0.12672	0.126846	0.01

**Table 10.** Moderate region windspeed profile at Kunming (25°N).

	$\Delta At$	$Fs^2$	$Fw^2$	$Ws_p^2$	$Fs^2, \Delta At$	$Fw^2, Ws_p^2$	$S$
January	-10.9	0.0144	0.0174	5.76	-0.15696	0.100224	-0.24
February	-11.2	0.0144	0.0174	8.41	-0.16128	0.146334	-0.12
March	-11	0.0144	0.0174	10.24	-0.1584	0.178176	0.14
April	-10.7	0.0144	0.0174	10.24	-0.15408	0.178176	0.15
May	-8.7	0.0144	0.0174	7.84	-0.12528	0.136416	0.10
June	-7.1	0.0144	0.0174	5.76	-0.10224	0.100224	-0.04
July	-6.2	0.0144	0.0174	4	-0.08928	0.0696	-0.14
August	-6.7	0.0144	0.0174	3.61	-0.09648	0.062814	-0.18
September	-7.3	0.0144	0.0174	4.00	-0.10512	0.0696	-0.19
October	-7.6	0.0144	0.0174	4.41	-0.10944	0.076734	-0.18
November	-9.2	0.0144	0.0174	4	-0.13248	0.0696	-0.25
December	-10.3	0.0144	0.0174	4.41	-0.14832	0.076734	-0.13

**Table 11.** Hot summer and cold region windspeed profile at Wuhan (30°N).

	$\Delta At$	$Fs^2$	$Fw^2$	$Ws_p^2$	$Fs^2, \Delta At$	$Fw^2, Ws_p^2$	$S$
January	-6.2	0.0144	0.0174	2.25	-0.08928	0.03915	-0.22
February	-7	0.0144	0.0174	2.56	-0.1008	0.044544	-0.24
March	-7.3	0.0144	0.0174	3.24	-0.10512	0.056376	-0.22
April	-8	0.0144	0.0174	3.61	-0.1152	0.062814	-0.23
May	-7.2	0.0144	0.0174	2.89	-0.10368	0.050286	-0.23
June	-6.4	0.0144	0.0174	2.89	-0.09216	0.050286	-0.20
July	-6.2	0.0144	0.0174	3.24	-0.08928	0.056376	-0.18
August	-6.1	0.0144	0.0174	3.61	-0.08784	0.062814	-0.16
September	-7.3	0.0144	0.0174	3.61	-0.10512	0.062814	-0.21
October	-7.3	0.0144	0.0174	2.56	-0.10512	0.044544	-0.25
November	-7.4	0.0144	0.0174	2.25	-0.10656	0.03915	-0.26
December	-7	0.0144	0.0174	2.56	-0.1008	0.044544	-0.24

**Table 12.** Hot summer and mild winter region windspeed profile at Haikou (20°N).

	$\Delta At$	$Fs^2$	$Fw^2$	$Ws_p^2$	$Fs^2, \Delta At$	$Fw^2, Ws_p^2$	$S$
January	-5.2	0.0144	0.0174	7.84	-0.07488	0.136416	0.24
February	-5.7	0.0144	0.0174	9.00	-0.08208	0.1566	0.27
March	-6.1	0.0144	0.0174	9.61	-0.08784	0.167214	0.28
April	-6.4	0.0144	0.0174	9.61	-0.09216	0.167214	0.27
May	-6.4	0.0144	0.0174	9.00	-0.09216	0.1566	0.25
June	-6.6	0.0144	0.0174	9.00	-0.09504	0.1566	0.25
July	-6.5	0.0144	0.0174	9.00	-0.0936	0.1566	0.25
August	-6	0.0144	0.0174	7.29	-0.0864	0.126846	0.20
September	-5	0.0144	0.0174	6.76	-0.072	0.117624	0.21
October	-4.9	0.0144	0.0174	7.84	-0.07056	0.136416	0.25
November	-4.8	0.0144	0.0174	9.00	-0.06912	0.1566	0.30
December	-4.7	0.0144	0.0174	9.00	-0.06768	0.1566	0.30

**Table 13.** Severe cold region weather profile at Harbin (44.5°N) with precipitation and temperature change pattern.

Month	At	$\bar{A}t_{max}$	$\bar{A}t_{min}$	RH	H_Gh	H_Bn	SDm	SDd	PCt	Pctd	Wsp	Wdr	$\Delta At$
January	-17.1	-11.9	-21.2	71	52	93	177	5.7	7	0	2.4	11	9.3
February	-11.3	-5.7	-16.7	64	74	109	191	6.8	3	1	2.7	11	11
March	-2.2	3.2	-7.2	50	119	141	234	7.5	10	1	3.3	11	10.4
April	8.5	14.2	3.1	43	140	116	221	7.4	10	3	3.4	184	11.1
May	15.8	21.6	9.8	45	163	118	254	8.2	32	4	3.3	154	11.8
June	21.6	26.4	15.3	53	168	124	249	8.3	44	7	2.9	174	11.1
July	23.7	27.9	19.3	71	156	113	238	7.7	50	11	2.6	153	8.6
August	21.4	25.7	17.1	73	139	114	231	7.5	60	8	2.3	174	8.6
September	15.6	21	9.8	62	119	116	225	7.5	30	6	2.4	11	11.2
October	6.3	11.8	1.7	55	88	111	211	6.8	18	3	2.8	11	10.1
November	-5.1	-0.4	-9.1	61	56	93	176	5.9	7	1	2.7	11	8.7
December	-14.5	-9.5	-18.8	68	43	74	155	5.0	4	1	2.5	11	9.3

**Table 14.** Cold region weather profile at Beijing (39.5°N) with precipitation and temperature change pattern.

Month	At	$\bar{A}t_{max}$	$\bar{A}t_{min}$	RH	H_Gh	H_Bn	SDm	SDd	PCt	Pctd	Wsp	Wdr	$\Delta At$
January	-3.4	-7.5	1.8	39	74	119	193	6.2	3	1	2.8	315	-9.3
February	0.6	-4.2	6	36	91	111	188	6.7	6	2	2.8	315	-10.2
March	7.1	1.9	12.8	36	132	132	235	7.6	9	2	3.1	315	-10.9
April	14.9	9.3	20.5	41	154	112	240	8.0	26	3	3	315	-11.2
May	20.7	14.9	26.4	49	184	121	276	8.9	29	4	2.8	295	-11.5
June	24.8	19.4	29.6	59	174	93	261	8.7	71	6	2.4	295	-10.2
July	27	22.7	31.5	70	155	79	219	7.1	176	10	2.1	90	-8.8
August	25.2	21.1	29.6	76	146	82	224	7.2	182	9	1.9	290	-8.5
September	20.7	15.6	25.7	66	132	105	236	7.9	49	4	2	290	-10.1
October	13	8.1	18.9	54	106	102	217	7.0	19	3	2.2	315	-10.8
November	4.6	0.2	9.7	50	73	94	185	6.2	6	1	2.4	315	-9.5
December	-1.4	-5.4	3.4	43	64	100	184	5.9	2	1	2.7	315	-8.8

**Table 15.** Moderate region weather profile at Kunming (25°N) with precipitation and temperature change pattern.

Month	At	Ātmax	Ātmin	RH	H_Gh	H_Bn	SDm	SDd	PCt	Pctd	Wsp	Wdr	ΔAt
January	9.5	4.4	15.3	58	115	141	222	7.2	22	2	2.4	279	-10.9
February	11.9	6.7	17.9	51	125	137	221	7.9	20	3	2.9	142	-11.2
March	15.2	10.1	21.1	47	159	142	255	8.2	30	3	3.2	142	-11
April	18.1	12.6	23.3	48	165	137	244	8.1	32	4	3.2	142	-10.7
May	19.2	14.9	23.6	60	154	97	214	6.9	90	9	2.8	142	-8.7
June	20.1	16.3	23.4	73	124	64	136	4.5	181	14	2.4	176	-7.1
July	20.1	17.1	23.3	78	121	63	139	4.5	175	16	2	142	-6.2
August	19.1	16.7	23.4	76	126	72	155	5.0	132	16	1.9	142	-6.7
September	18.2	14.5	21.8	72	112	82	135	4.5	80	12	2	279	-7.3
October	16.2	12.5	20.1	74	101	66	149	4.8	88	11	2.1	279	-7.6
November	12.4	7.9	17.1	69	100	99	172	5.7	29	5	2	279	-9.2
December	9.3	4.7	15	67	104	136	199	6.4	22	2	2.1	279	-10.3

**Table 16.** Hot summer and cold winter region weather profile at Wuhan (30°N) with precipitation and temperature change.

Month	At	Ātmax	Ātmin	RH	H_Gh	H_Bn	SDm	SDd	PCt	Pctd	Wsp	Wdr	ΔAt
January	4.6	1.7	7.9	71	62	43	91	2.9	67	5	1.5	198	-6.2
February	7.6	4.2	11.2	68	67	29	80	2.9	63	6	1.6	23	-7
March	11.7	8.3	15.6	70	86	34	99	3.2	89	9	1.8	81	-7.3
April	18.2	14.1	22.1	70	107	40	122	4.1	135	11	1.9	81	-8
May	22.9	19.5	26.7	71	138	60	147	4.7	166	11	1.7	81	-7.2
June	26.5	22.9	29.3	75	135	49	160	5.3	171	10	1.7	81	-6.4
July	29.4	26.2	32.4	75	165	90	209	6.7	202	10	1.8	110	-6.2
August	28.2	25.3	31.4	76	150	87	213	6.9	117	10	1.9	81	-6.1
September	24.8	20.8	28.1	70	116	59	148	4.9	57	8	1.9	66	-7.3
October	18.6	15.1	22.4	71	93	57	132	4.3	80	8	1.6	66	-7.3
November	12.4	8.7	16.1	71	70	54	112	3.7	80	6	1.5	212	-7.4
December	6.4	3.3	10.3	70	62	44	101	3.3	39	4	1.6	198	-7

**Table 17.** Hot summer and mild winter region weather precipitation profile at Haikou (20°N)

Month	At	Ātmax	Ātmin	RH	H_Gh	H_Bn	SDm	PCt	Pctd	Wsp	Wdr	SDd	ΔAt
January	20.1	17.6	22.8	77	97	70	123	15	4	2.8	181		-5.2
February	20.2	17.4	23.1	80	89	42	101	44	6	3	119		-5.7
March	22.6	19.8	25.9	83	116	58	140	45	6	3.1	124		-6.1
April	25.5	22.1	28.5	83	131	60	170	68	8	3.1	124		-6.4
May	27.1	24	30.4	84	171	114	224	117	12	3	119	7	-6.4
June	28.3	24.7	31.3	82	167	116	219	162	12	3	136	7	-6.6
July	28.8	25.6	32.1	80	175	120	254	247	11	3	225	8	-6.5
August	28.7	25.8	31.8	80	169	113	220	276	12	2.7	121	7	-6
September	27.8	25.1	30.1	80	132	73	194	313	12	2.6	181	6	-5
October	26.9	24.6	29.5	75	122	69	184	162	10	2.8	181	5	-4.9
November	24.2	21.6	26.4	74	103	69	148	46	6	3	176	4	-4.8
December	20.8	18.6	23.3	73	93	66	141	48	4	3	176	4	-4.7

**Table 18.** Year-round infiltration pattern across regions.

Regions	Infiltration Rate	
	Maximum	Minimum
Hot summer and Mild Winter	November December	September
Hot summer and Cold winter	August	November,
Severe cold	April	August
Cold	March	September
Moderate	April	September

**Table 19.** Thermal profiling and infiltration pattern across regions.

Regions	Passive Solar gains	Thermal Capacity	Air tightness	Passive Solar Controls	Ventilation	Infiltration Rate	
						Maximum	Minimum
Severe cold	√	√	√	-	-	November December	September
Cold	√	√	√	√	√	August	November,
Moderate	-	-	-	√	√	April	August
Hot Summer and Cold Winter	√	√	√	√	√	March	September
Hot Summer and Warm winter	-	-	-	√	√	April	September

**Table 20.** Solar radiative values across China’s climate regions.

S/N	Region	$H_{-Gh}$	Parameters	$H_{-Bn}$
1.	Severe Cold Region	1315	0.74	1321
2.	Cold Region	1484	0.71	1249
3.	Moderate	1506	0.73	1236
4.	Hot summer cold winter	1249	0.71	646
5.	Hot Summer mild winter	1561	0.76	970

As a measure of wattage per square meter, solar radiations are sources of thermal gain in buildings. The amount it impacts on the wall towards finding its admittance into the building is a function of the construction material used. Deductively and in line with investigation, Vernacular buildings in severe cold regions with the highest solar admittance are compensated by nature with many thermal gains on the basis of the vernacular floor area, U-value factor and temperature differential between outer and inner wall skin [54].

## 6. Conclusions

In this paper, the investigation was conducted to

profile the pattern of air leakage by infiltration in Chinese vernacular buildings in the thinking to adopt Chinese architectural concepts into modern designs for energy minimization needs from their psychrometric and sensible heat properties with respect to climate profiles. From the data provided on a yearly basis, it was observed that in the five climate regions where these vernacular buildings are spread across China, their pattern of minimums and maximums at certain times of the year is conversely related to their design features. Some regions have shown similarities with respect to pattern for example, hot summer and mild winter regions have their highest infiltration rate in November/December and lowest in Sep-



tember which also cold and moderate regions have too. By means of the Angstrom estimation model, this paper presents us with the findings of radiative admittance value into Chinese vernacular buildings towards understanding the varying psychrometric occupants' comfort patterns on a yearly basis across the five climate regions of China. Accordingly, data showed that solar radiation admittance is highest at buildings in severe cold regions. This implies that earlier Chinese were able to cope with cold temperatures on the basis of higher radiative admittance in spite of the severity of the region's coldness. This is intrinsically linked to their survival compensation by nature in the region that ordinarily will need internal supportive heating. This again underscores the impact on the occupants if all regions were to be having equal admittance levels.

#### Recommendation

Following the findings from this research, it is recommended that Chinese architectural design features should be mimicked and adapted in modern architectural thinking in the best interest of energy demand minimization and sustainability. This is spurred by the Vernacular building's potential to compensate for energy lack by natural admittance all year round according to their architectural designs.

### List of symbols

$\bar{A}_{\min}$	=	air temperature (°C)
$A_{\max}$	=	mean daily minimum air temperature
$R_H$	=	relative humidity
$H_{G_h}$	=	irradiation of global radiation horizontal
$H_{B_n}$	=	irradiation of solar beam (Kwh/M <sup>2</sup> )
$SD_m$	=	sunshine duration (monthly)
$SD_d$	=	sunshine duration daily (hours)
$PC_t$	=	precipitation (mm)
$PC_{td}$	=	days with precipitation
$W_{sp}$	=	windspeed (m/s)
$W_{dr}$	=	wind direction (°C)

### Conflict of Interest

There is no conflict of interest.

### Acknowledgement

The authors are indebted to Dr. Feifei Sun of NPS group, Earle House, Colonial Street, Kingston Upon Hull, HU28JY, UK and in association with Beijing Institute of China Construction and Design for data on Meteonorm V 6.1.

### References

- [1] Hou, R., 2014. Khanbaliq (1267-1368) of the Yüan Dynasty (1260-1368). An historical geography of Peiping. Springer: Berlin. pp. 75-94. DOI: [https://doi.org/10.1007%2F978-3-642-55321-9\\_7](https://doi.org/10.1007%2F978-3-642-55321-9_7)
- [2] Jin, X., Zhang, X., Cao, Y., et al., 2012. Thermal performance evaluation of the wall using heat flux time lag and decrement factor. *Energy and Buildings*. 47, 369-374.
- [3] Hagra, H., 2017. An ancient mosque in Ningbo, China "historical and architectural study". *Journal of Islamic Architecture*. 4(3), 102-113.
- [4] Jin, X., Chiou, S.C., 2015. Architectural features and preservation of ancient residential complexes of the changs in Xiangnan, Xiamen. *International Archives of the Photogrammetry, Remote Sensing & Spatial Information Sciences*. XL-5/W7, 453-460.
- [5] Aldawould, A., Clark, R., 2008. Comparative analysis of energy performance between courtyard and atrium in buildings. *Energy and Buildings*. 40(3), 209-214.
- [6] Zamani, Z., Heidari, S., Hanachi, P., 2018. Reviewing the thermal and microclimatic function of courtyards. *Renewable and Sustainable Energy Reviews*. 93, 580-595.
- [7] Hagra, H., 2017. An ancient mosque in Ningbo, China: Historical and architectural study. *Journal of Islamic Architecture*. 4(3), 102-113.
- [8] Hagra, H., 2019. Xi'an Daxuexi Alley Mosque: Historical and architectural study. *Egyptian Journal of Archaeological and Restoration Studies*. 1, 97-113.
- [9] Wang, X., Li, Z., Zhang, L., 2010. Condition Conservation and Reinforcement of the Yumen

- Pass and Hecang Earthen Ruins New Dunhuang. Conservation of Ancient Sites on the Silk Road: Proceedings of the Second International Conference on the Conservation of Grotto Sites, Mogao Grottoes, Dunhuang, China; 2004 June 28-July 3; Los Angeles: The Getty Conservation Institute. p. 351-357.
- [10] Li, L., Tang, L., Zhu, H., et al., 2017. Semantic 3D modeling based on CityGML for ancient Chinese-style architectural roofs of digital heritage. *International Journal of Geo-Information*. 6(5), 132.
- [11] Cho, J., Yoo, C., Kim, Y., 2014. Viability of exterior shading devices for highrise buildings: Case Study for cooling energy savings and economic feasibility analysis. *Energy and Buildings*. 82, 771-785.
- [12] Liu, Y., Tan, Q., Pan, T., 2019. Determining the parameters of the Ångström-Prescott model for estimating solar radiation in different regions of China: Calibration and modeling. *Earth and Space Science*. 6(10), 1976-1986.  
DOI: <https://doi.org/10.1029.2019EA00635>
- [13] Sadafi, N., Elias, S., Lim, C.H., et al., 2011. Evaluating thermal effects of internal courtyard in a tropical terrace house by computational simulation. *Energy and Buildings*. 43(4), 887-893.  
DOI: <https://doi.org/10.1016/j.enbuild.2010.12.009>
- [14] James-Chakraborty, K., 2014. Ming and Qing China. *Architecture since 1400*. University of Minnesota Press: Minneapolis. pp. 1-15.
- [15] Aversa, P., Palumbo, D., Donatelli, A., et al., 2017. Infrared thermography for the investigation of dynamic thermal behaviour of opaque building elements: Comparison between empty and filled with hemp fibres prototype walls. *Energy and Buildings*. 152, 264-272.  
DOI: <https://doi.org/10.1016/J.Enbuild.2017.07.055>
- [16] Zheng, S., Han, B., Wang, D., et al., 2018. Ecological wisdom and inspiration underlying the planning and construction of ancient human settlements: Case study of hongcun UNESCO world heritage site in China. *Sustainability*. 10(5), 1345.
- [17] Ren, H.B., 2000. Feng Shui and Chinese Traditional Domestic Architecture. [Master's Thesis]. Cincinnati: University of Cincinnati.
- [18] Sun, F., 2013. Chinese climate and vernacular dwellings. *Buildings*. 3(1), 143-172.
- [19] Baoping, X., Lin, F., Hongfa, D., 2008. Dynamic simulation of space heating systems with radiators controlled by TRVs in buildings. *Energy and Buildings*. 40(9), 1755-1764.  
DOI: <https://doi.org/10.1016/j.enbuild.2008.03.004>
- [20] Zhuang, Z., Li, Y., Chen, B., et al., 2009. Chinese Kang as a domestic heating system in rural northern China—A review. *Energy and Buildings*. 41(1), 111-119.
- [21] Zhang, Y., Li, X., Bai, Y., 2015. An integrated approach to estimate shortwave solar radiation on clear-sky days in rugged terrain using MODIS atmospheric products. *Solar Energy*. 113, 347-357.  
DOI: <https://doi.org/10.1016/j.solener.2014.12.028>
- [22] Chen, Y., Athienitis, A.K., Galal, K., 2012. Thermal performance and charge control strategy of a ventilated concrete slab (VCS) with active cooling using outdoor air. *ASHRAE Transactions*. 118(2), 556-568.
- [23] Martínez-Garrido, M.I., Aparicio, S., Fort, R., et al., 2014. Effect of solar radiation and humidity on the inner core of walls in historic buildings. *Construction and Building materials*. 51, 383-394.
- [24] Ge, J., Li, S., Chen, S., et al., 2021. Energy-efficiency strategies of residential envelope in China's Hot Summer-Cold Winter Zone based on intermittent thermal regulation behaviour. *Journal of Building Engineering*. 44, 103028.  
DOI: <https://doi.org/10.1016/j.jobee.2021.103028>
- [25] Kim, Y.M., 2017. Virtual pilgrimage and virtual geography: Power of Liao Miniature Pagodas (907-1125). *Religions*. 8(10), 206.
- [26] Nagy, B., Nehme, S.G., Szagri, D., 2015. Thermal properties and modeling of fiber reinforced

- concretes. *Energy Procedia*. 78, 2742-2747.  
DOI: <https://doi.org/10.1016/J.Egypro.2015.11.616>
- [27] Goodrich, L.C., 2002. A short history of the Chinese people. Courier Corporation: North Chelmsford.
- [28] Roman, K.K., O'Brien, T., Alvey, J.B., et al., 2016. Simulating the effects of cool roof and PCM (phase change materials) based roof to mitigate UHI (urban heat island) in prominent US cities. *Energy*. 96, 103-117.  
DOI: <https://doi.org/10.1016/J.Energy.2015.11082>
- [29] Kandya, A., Mohan, M., 2018. Mitigating the urban heat island effect through building envelope modifications. *Energy and Buildings*. 164, 266-277.  
DOI: <https://doi.org/10.1016/J.Enbuild.2018.01.014>
- [30] Andoni, H., Jurizat, A., Steven, S., et al., 2018. Thermal behaviour studies on building walls based on type and composition of the materials. *IOP Conference Series: Materials Science and Engineering*. 547, 012058.
- [31] Aversa, P., Palumbo, D., Donatelli, A., et al., 2017. Infrared thermography for the invention of dynamic thermal behavior of opaque building element: Comparison between empty and filled with hemp fibress prototype walls. *Energy and Buildings*. 152, 264-272.  
DOI: <https://doi.org/10.1016/J.Enbuild.2017.07.055>
- [32] Nagy, B., Nehme, S.G., Szagri, D., 2015. Thermal properties and modeling of fiber reinforced concretes. *Energy Procedia*. 78, 2742-2747.  
DOI: <https://doi.org/10.1016/J.Egypro.2015.11.616>
- [33] Andoni, H., Jurizat, A., Thomas, D., et al., 2019. Thermal Behaviour Studies on Building Walls Based on Type and Composition of The Materials. *IOP Conf. Ser.: Materials Science and Engineering*. 547(1), 012058
- [34] Ahmed, A.Y.F., 2019. Advances in passive cooling design: An integrated design approach. *Zero and net zero energy*. Intech Open: London.
- [35] Oropeza-Perez, I., Østergaard, P.A., 2018. Active and passive cooling methods for dwellings: A review. *Renewable and Sustainable Energy Reviews*. 82, 531-544.
- [36] Panchabikesan, K., Vellaisamy, K., Ramalingam, V., 2017. Passive cooling potential in buildings under various climatic conditions in India. *Renewable and Sustainable Energy Reviews*. 78, 1236-1252.
- [37] Tejero-González, A., Andrés-Chicote, M., García-Ibáñez, P., et al., 2016. Assessing the applicability of passive cooling and heating techniques through climate factors: An overview. *Renewable and Sustainable Energy Reviews*. 65, 727-742.
- [38] Prieto, A., Knaack, U., Auer, T., et al., 2018. Passive cooling & climate responsive façade design: Exploring the limits of passive cooling strategies to improve the performance of commercial buildings in warm climates. *Energy and Buildings*. 175, 30-47.
- [39] U.S Department of Energy, 1992. *Fundamentals Handbook Thermodynamics, Heat Transfer, and Fluid Flow Vol. 1-3* [Internet]. DOE-HDBK-1012/1-92. DOE: Washington, DC. Available from: <https://www.steamtableonline.com/pdf/Thermodynamics-Volume1.pdf>
- [40] Xie, C., 2012. Interactive heat transfer simulations for everyone. *The Physics Teacher*. 50(4), 237-240.  
DOI: <https://doi.org/10.1119/1.3694080>
- [41] Zhou, A., Wong, K.W., Lau, D., 2014. Thermal insulating concrete wall panel design for sustainable built environment. *The Scientific World Journal*. Article ID 279592.  
DOI: <https://doi.org/10.1155/2014/279592>
- [42] Medved, S., 2022. Heat transfer in buildings structures and thermal comfort in buildings. *Building physics*. Springer, Cham.: Berlin.  
DOI: [https://doi.org/10.1007/978-3-030-74390-1\\_1](https://doi.org/10.1007/978-3-030-74390-1_1)
- [43] Kreider, J.F., Rabl, A., 1994. *Heating and cooling of buildings: Design for efficiency*. McGraw-Hill Publishing: New York.
- [44] Kachkouch, S., Ait-Nouh, F., Benhamou, B., et al., 2018. Experiment assessment of thermal performance of three passive cooling techniques for roofs in a semi-arid climate. *Energy and Buildings*. 164, 153-164.

DOI: <https://doi.org/10.1016/j.enbuild.2018.01.008>

[45] Max, S., 2017. Infiltration in ASHRAE's Residential Ventilation Standards [Internet]. Available from: <https://www.osti.gov/servlets/purl/943513>

[46] Wang, L., Kisi, O., Zounemat-Kermani, M., et al., 2016. Solar radiation prediction using different techniques: Model evaluation and comparison. *Renewable & Sustainable Energy Reviews*. 61, 384-397.  
DOI: <https://doi.org/10.1016/j.rser.2016.04.024>

[47] Gowri, K., Winiarski, D., Jarnagin, R., 2009. Infiltration modelling guidelines for commercial building energy analysis. U.S. Department of Energy. Contract DE-AC05-76RLO1830, PNNL-18898. Available from: [https://www.pnnl.gov/main/publications/external/technical\\_reports/PNNL-18898.pdf](https://www.pnnl.gov/main/publications/external/technical_reports/PNNL-18898.pdf)

[48] Chan, W.R., Joh, J., Sherman, M.H., 2012. Analysis of Air leakage measurements for residential diagnostics database. Ernest Orlando Lawrence Berkeley National Laboratory. Environmental Energy Technology Division. Available from: <https://www.osti.gov/servlets/purl/1163524/>

[49] Zhao, J., 1995. China natural geography (third edition). Higher Education Press: Beijing.

[50] Sanchez-Lorenzo, A., Enriquez-Alonso, A., Wild, M., et al., 2017. Trends in downward surface solar radiation from satellites and ground observations over Europe during 1983-2010. *Remote Sensing of Environment*. 189, 108-117.  
DOI: <https://doi.org/10.1016/j.rse.2016.11.018>

[51] Qin, J.C., Yang, K., Liang, S., et al., 2011. Estimation of monthly-mean daily global solar radiation baseil on modis and tromm products. *Applied Energy*. 88(7), 2480-2189.  
DOI: <https://doi.org/10.1016/j.apenergy.2011.01.018>

[52] Zhao, N., Zeng, X., Han, S., 2013. Solar radiation estimation using sunshine hour and air pollution index in China. *Energy Conversion and Management*. 76, 846-851.  
DOI: <https://doi.org/10.1016/j.enconman.2013.08.037>

[53] Yacef, R., Mellit, A., Belaid, S., et al., 2014.

New combined models for estimating daily global solar radiation from measured air temperature in semi-arid climates: Application in GhardaTa, Algeria. *Energy Conversion & Management*. 79, 606-615.

DOI: <https://doi.org/10.1016/j.eneonman.2013.12.057>

[54] Rensheng, C., Shihua, L., Ersi, K., et al., 2006. Estimating daily global radiation using two types of revised models in China. *Energy Conversion and Management*. 47(7-8), 865-878.

DOI: <https://doi.org/10.1016/j.enconman.2005.06.015>

## Appendix

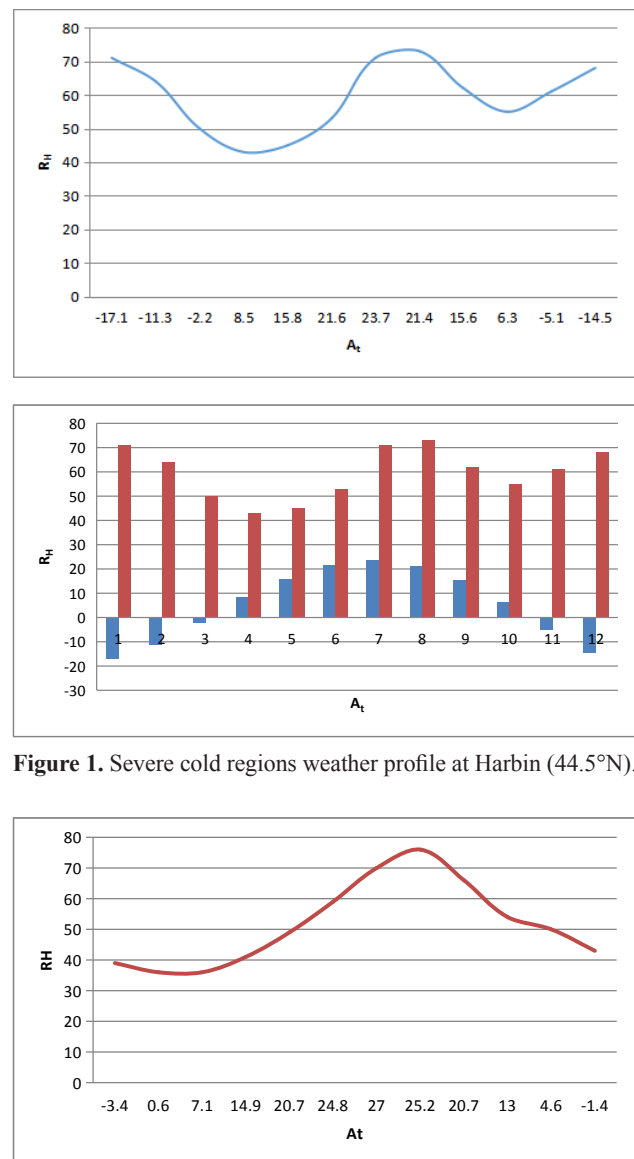


Figure 1. Severe cold regions weather profile at Harbin (44.5°N).

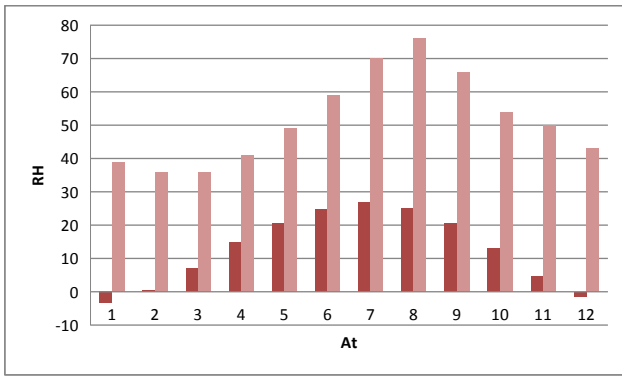


Figure 2. Severe cold region weather profile at Beijing (39.5°N).

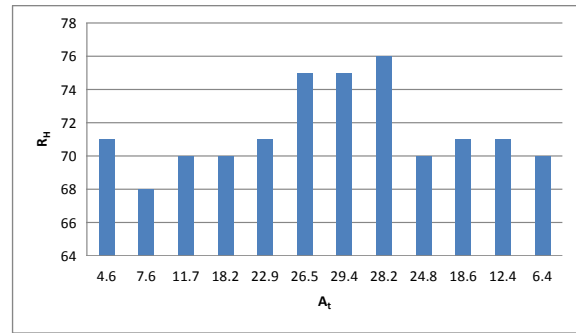


Figure 4. Hot summer and cold winter region weather profile at Wuhan (30°N).

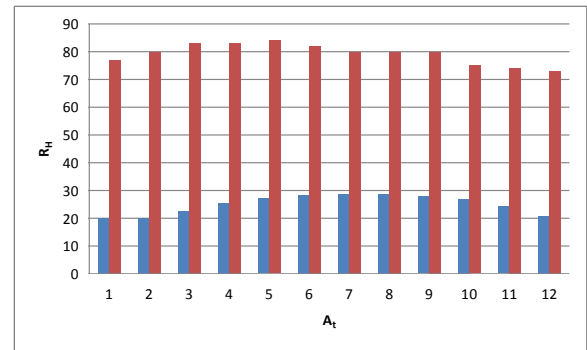
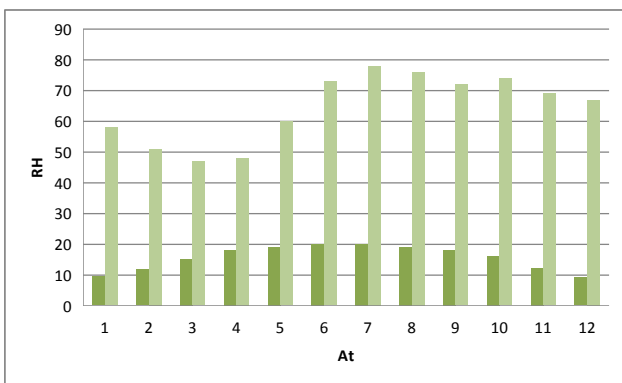
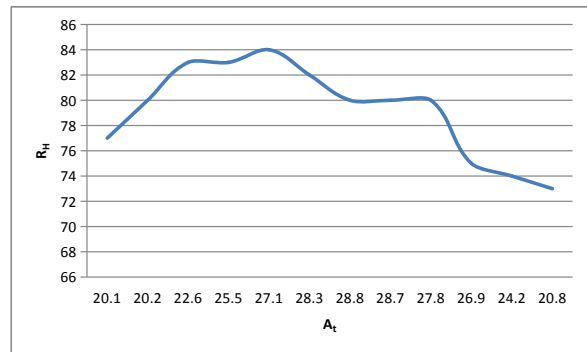
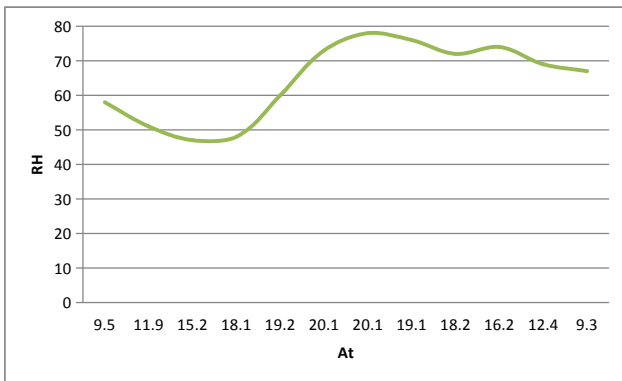


Figure 3. Moderate region weather profile at Kunming 25°N.

Figure 5. Hot summer and mild winter region weather profile at Haikou (20°N).

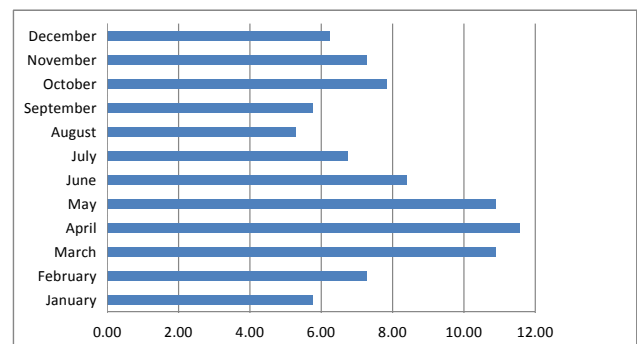
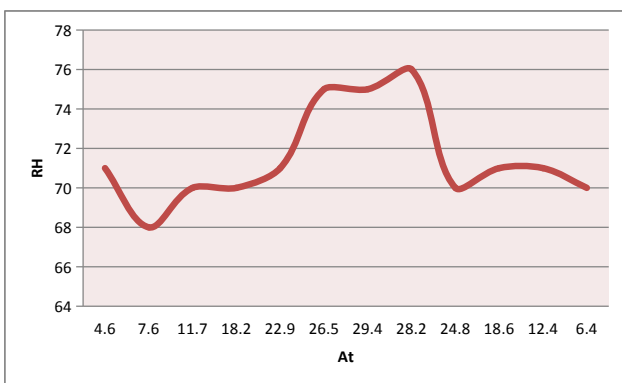


Figure 6. Severe cold region windspeed profile at Harbin (44.5°N).

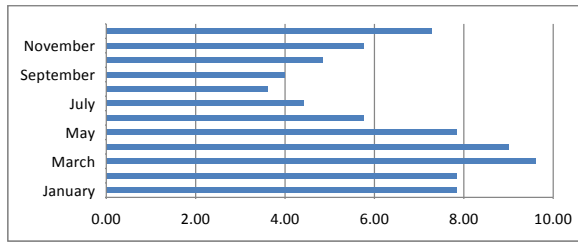


Figure 7. Severe cold region windspeed profile at Beijing (39.5°N).

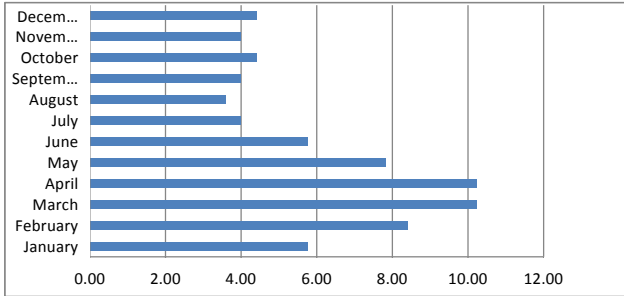


Figure 8. Moderate region windspeed profile at Kunming (25°N).

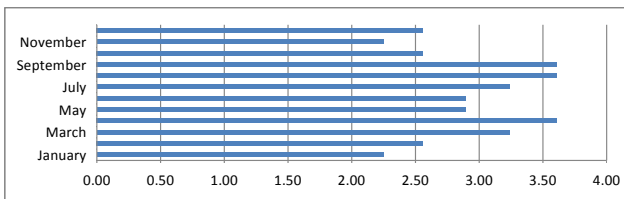


Figure 9. Hot summer and cold region windspeed profile at Wuhan (30°N).

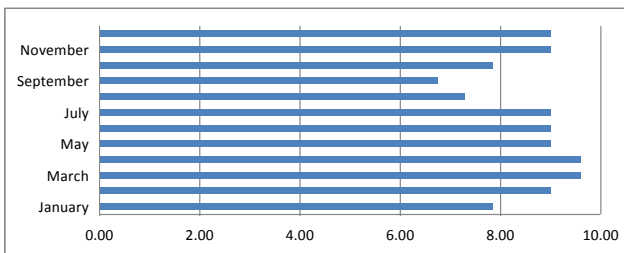


Figure 10. Hot summer and mild winter region windspeed profile at Haikou (20°N).

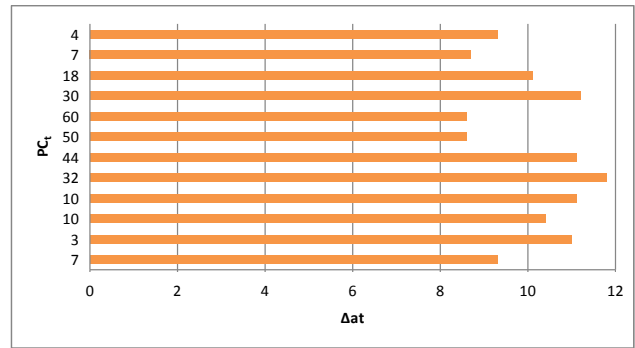
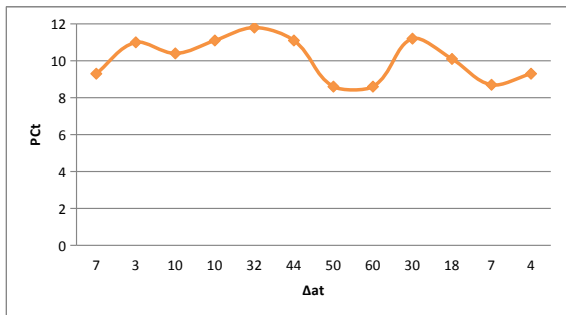


Figure 11. Severe cold region weather profile at Harbin (44.5°N) with precipitation and temperature change pattern.

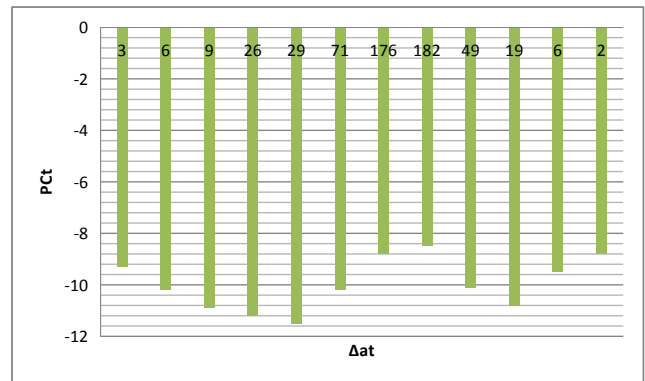
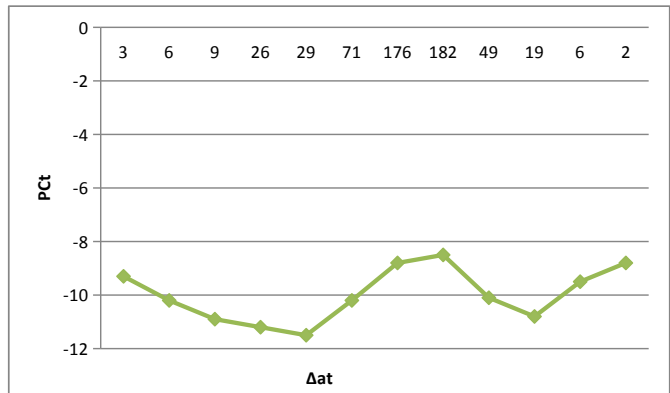
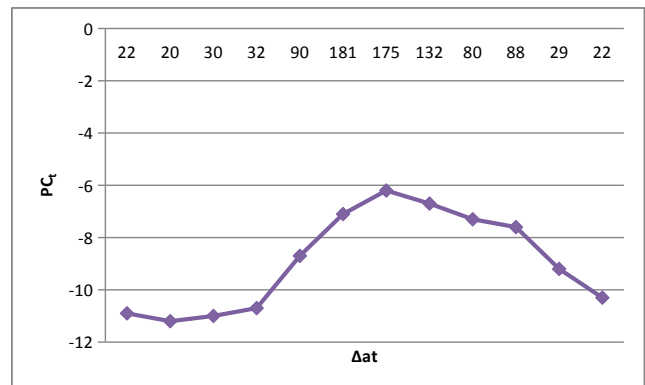


Figure 12. Cold region weather profile at Beijing (39.5°N) with precipitation and temperature change pattern.



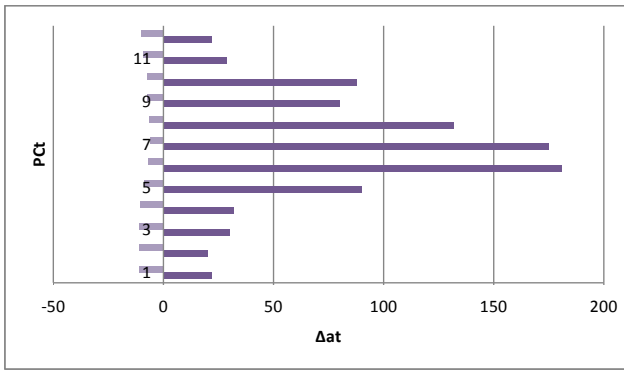


Figure 13. Moderate region weather profile at Kunming (25°N) with precipitation and temperature change pattern.

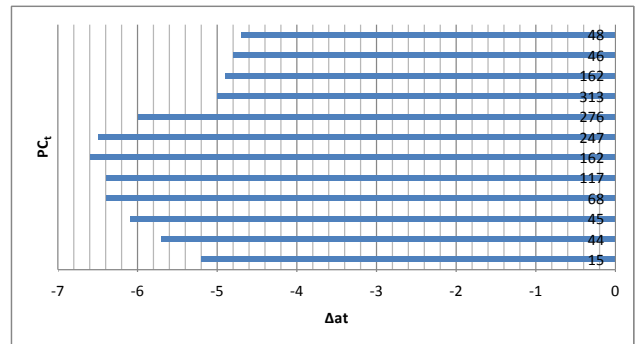
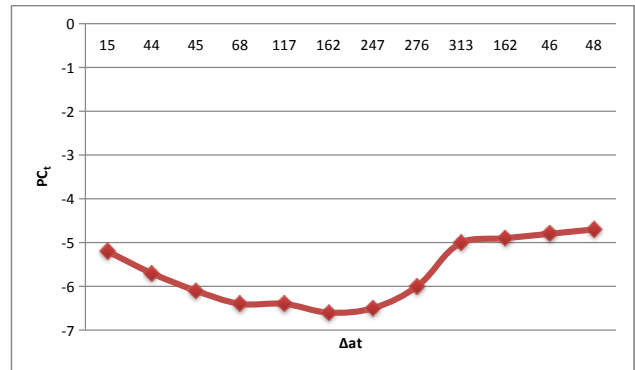


Figure 15. Hot summer and mild winter region weather precipitation profile at Haikou (20°N).

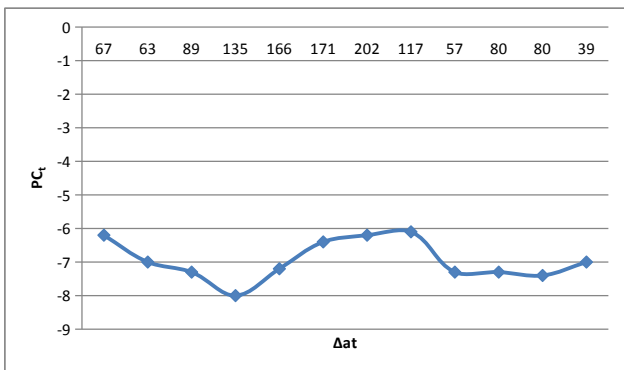


Figure 14. Hot summer and cold winter region weather profile at Wuhan (30°N) with precipitation and temperature change.

